

The nitrogen-to-oxygen evolution in galaxies: the role of the star formation rate

M. Mollá,^{1*} J. M. Vílchez,² M. Gavilán³ and A. I. Díaz³

¹*Departamento de Investigación Básica, CIEMAT, Avda. Complutense 22, 28040 Madrid, Spain*

²*Instituto de Astrofísica de Andalucía (CSIC), Apdo. 3004, 18080 Granada, Spain*

³*Departamento de Física Teórica, Universidad Autónoma de Madrid, 28049 Cantoblanco, Madrid, Spain*

Accepted 2006 July 31. Received 2006 July 13; in original form 2006 April 10

ABSTRACT

The main objective of this work is to check if the star formation efficiency plays a relevant role in the evolution of the relative abundance N/O. In order to explore this idea, we analyse the evolution of the nitrogen-to-oxygen ratio as predicted by a set of computed theoretical models. These models consist of simulated galaxies with different total masses which are evolved assuming different collapse time-scales and different star formation efficiencies. The combinations of these two parameters produce different star formation histories, which in turn have, as we show, an important impact on the resulting N/O ratio. Since we want to check the effect of variations in these efficiencies on our model results, the same stellar yield sets are used for all of them. The selected yields have an important primary nitrogen contribution coming from low- and intermediate-mass stars, which implies that N is ejected with a certain delay with respect to O. It allows us to obtain, as we demonstrate, a dispersion of results in the N/O–O/H plane when star formation efficiencies vary which is in general agreement with observations. The model results for the N/O abundance ratio are in good agreement with most observational data trends. In particular, the behaviour shown by the extragalactic H II regions is well reproduced with present-time resulting abundances. Furthermore, the low N/O values estimated for high-redshift objects, such as those obtained for damped Lyman α galaxies, as well as the higher (and constant) values of N/O observed for irregular and dwarf galaxies or halo stars, can be simultaneously obtained with our models at the same low oxygen abundances $12 + \log(\text{O}/\text{H}) \sim 7$. We therefore conclude that, even though there seems to be a general belief that abundance ratios depend mostly on stellar yields, these are not the only parameter at work when both elements are ejected by stars of different mass ranges, and that differences in the star formation history of galaxies and regions within them are a key factor to explain the data in the N/O–O/H plane.

Key words: galaxies: abundances – galaxies: dwarf – galaxies: evolution – galaxies: irregular – galaxies: spiral – galaxies: stellar content.

1 INTRODUCTION

Nitrogen abundances have posed an important debate which lasts up to now. First, because it is created in two types of stars, which raises doubt about what proportion is produced in massive stars and how much N is ejected by low- and intermediate-mass (LIM) stars. Secondly, the possible primary or secondary origin of nitrogen implies some questions about what is the contribution of each type produced in each star. The question is then how much N is created in each stellar mass range and what fraction of it is primary?

From an observational point of view, the need for a primary component of N appeared very soon. Edmunds & Pagel (1978) and Alloin et al. (1979) already concluded, from the analysis of the then available extragalactic H II region data, that N behaves, at least partially, as a primary element. This was later supported by N measurements for Galactic metal-poor halo stars (Barbuy 1983; Tomkin & Lambert 1984; Laird 1985; Carbon et al. 1987), and by additional extragalactic H II region observations (McCall, Rybski & Shields 1985; Vila Costas & Edmunds 1993). The number of N data points has increased extraordinarily since then (see Henry, Edmunds & Köppen 2000; Contini et al. 2002, and references therein) showing the same basic trend: (1) a strong slope for the N/O data against oxygen abundance for metal-rich regions, a well-explained behaviour by

*E-mail: mercedes.molla@ciemat.es

the secondary character expected from the CNO cycle production, and (2) a flat line for the data of low-mass and irregular galaxies and halo stars with $12 + \log(\text{O}/\text{H}) < 8$. Some very recent observations of halo stars (Israelian et al. 2004; Spite et al. 2005) have increased the number of data in the low-abundance end. They show a large scatter in N/O at low metallicities, and some high N/O ratios, implying an important primary N production at very early evolutionary times.

Since low-metallicity galaxies have been considered to be young objects undergoing their first burst of star formation (Thuan, Izotov & Lipovetsky 1995), it was assumed that they have had no time for their LIM stars to evolve and eject the nitrogen produced by them. Moreover, the dispersion found for their N/O abundances was really low. This way, a number of authors have claimed that massive stars are the main primary N producers. There are two facts against this argument: (1) these galaxies are not so young as it was thought, since recent observations indicate that they host stellar populations which are at least 10^7 – 10^8 yr old, reaching even 1 Gyr in some cases (Legrand 2000; Cairós et al. 2003; Tolstoy 2003; van Zee, Barton & Skillman 2004; Thuan & Izotov 2005); (2) if LIM stars with masses in the range 4 – $8 M_{\odot}$ eject some amount of the primary N, this can be in the interstellar medium (ISM) within a time as short as $\sim[50$ – $200]$ Myr, since the mean-lifetimes of these stars are in this range. Moreover, low oxygen abundances do not necessarily imply short time-scales. In fact, we claim that it is essential to change the usual scheme that identifies oxygen abundances with evolutionary time, a misunderstanding that can lead to erroneous conclusions.

On the other hand, there is no clear mechanism that may produce primary N in massive stars. Some authors working on stellar evolution have searched for new possibilities, the most plausible one being the effect of rotation on stars. Meynet & Maeder (2002) have computed some yields from stellar models including rotation, obtaining that intermediate and massive stars may produce primary N, mostly at very low metallicity. However, Chiappini, Matteucci & Ballero (2005) have included these yields in a Galactic chemical evolution (GCE) model, finding that an extra-production of N in low-metallicity massive stars by a large factor of between 40 and 200 along the mass range is still necessary to explain the data for very metal-poor halo stars, since the yields used do not produce a sufficient amount of the primary N. Recently, Chiappini et al. (2006) use new (and still unpublished) yields for metal-poor massive stars which rotate rapidly, thus producing large amounts of the primary nitrogen, with which it is possible to increase the N/O abundance up to levels similar to those of the Galactic halo stars. These preliminary yields are still uncertain, since they are computed assuming a non-observed very high rotation velocity for these low-metallicity stars.¹

The situation has become more complicated because abundances of N for damped Lyman α (DLA) galaxies have been derived (Pettini et al. 2002; Prochaska et al. 2002; Centurión et al. 2003, and references therein). When these recent observations are included in the sample, a large dispersion appears, in evident disagreement with the hypothesis that all the primary N is produced by massive stars. DLA data show lower values of N/O than those, populating the flat slope, obtained for the irregular and blue compact galaxies and for the halo stars of similar oxygen abundance. These high-redshift objects have oxygen abundances which correspond to slightly evolved

objects such as those observed in the local Universe, but in this case some values of N/O are much smaller than the local ones. This fact appears incompatible with the primary N being produced by massive stars, such as those very metal-poor ones rotating at very high velocity used in Chiappini et al. (2006), since in that case it is difficult to conceive which mechanism could produce a different final yield (and therefore a different point on the N/O–O/H plane) for each DLA object.

From the theoretical point of view, a secondary production is expected in most stars, which would correspond to the CNO cycle, while the primary contribution should arise from intermediate-mass stars ($4 \leq M/M_{\odot} \leq 8$). These stars may suffer, during the asymptotic giant branch (AGB) phase, dredge-up episodes and hot bottom burning (HBB) processes, due to which some primary N may be created. This fact has been well known for some decades (Renzini & Voli 1981; Serrano 1986). In fact, most yield sets (such as van den Hoek & Groenewegen 1997; Marigo, Bressan & Chiosi 1998) presently used for the chemical evolution models include a primary N contribution produced by these processes in LIM stars. The AGB phase is still far from being well understood, and there exist large uncertainties about the exact amount of primary nitrogen produced through the HBB process. Probably due to that reason, the up-to-now computed models do not seem to be able to reproduce most of the data.

The idea that a constant N/O may only be obtained with primary N from massive stars is indeed an oversimplification which does not take into account the stellar lifetimes. Vila Costas & Edmunds (1993) and Pilyugin, Thuan & Vilchez (2003), by analysing the N/O values in galaxies of different morphological types, concluded that a long-time-delayed contribution to the N production must exist. Vila Costas & Edmunds (1993) suggested that most data fall in a region limited by two extreme closed box models (CBMs) defined by distinct delays, produced by different star formation efficiencies, and/or ages of galaxies, thus explaining the observed dispersion.

This way, Henry et al. (2000) and Prantzos (2003) – hereafter HEN and PRAN, respectively – computed realistic chemical evolution models using yields from van den Hoek & Groenewegen (1997) for LIM stars, with a primary N contribution. Although their models produce a level of N/O higher than observations for low Z , they show that, actually, a N/O–O/H relation much flatter than usual may be obtained with their models, only decreasing the efficiencies of star formation. The same finding was also obtained by Larsen, Sommer-Larsen & Pagel (2001) using several sets of yields, all of them with a proportion of primary N ejected by LIM stars. These results led to the idea that stellar yields are not the only driver of the N/O ratio, at least when LIM stars produce a quantity of the primary N, and that most observations in the plot N/O–O/H might be reproduced if different star formation rates (SFRs) in the different galaxies or regions are considered.

Gavilán, Buell & Mollá (2005) and Gavilán, Mollá & Buell (2006), hereafter GAV05 and GAV06, respectively, have recently calculated some chemical evolution models for the Milky Way Galaxy (MWG), by using different sets of stellar yields. They demonstrated in those works that a model using the set of yields for LIM stars from GAV05 combined with the massive stellar yields from Woosley & Weaver (1995, hereafter WW) is able to reproduce most of the trends of MWG data. In the cited model, a flat behaviour of N/O versus O/H appears when the SFR is low during a long time, as occurs in the Galactic halo or in the outer regions of the Galactic disc. In this case, since the evolution is slow, a time longer than 40 Myr is necessary to reach oxygen abundances $12 + \log(\text{O}/\text{H}) \sim 7$, which is sufficient for LIM stars to eject their products to the ISM.

¹ In fact, as Hirschi (2005) stated, the ratio v_{ini}/v_c decreases at very low metallicity for the initial velocity of 300 km s^{-1} , because stars are more compact at lower metallicity.

This, combined with low O/H abundances, produces high N/O values similar to those observed for low abundances. Most of the data of the Galaxy halo and disc, in particular those of nitrogen – see fig. 12 of GAV06 – are successfully reproduced with that model. Furthermore, the model results for the radial regions other than the solar neighbourhood suggest that actually the dispersion observed in MWG data can be a consequence of different star formation histories (produced by different collapse time-scales to form the disc and different efficiencies to form stars) in the Galactic radial regions. This supports the mentioned findings from the above cited authors: different evolutionary tracks and end points in the O/H–N/O plane are possible simply by increasing or decreasing the SFR, although other parameters probably also play a role.

The objective of this work is, therefore, to explore if different star formation efficiencies may produce different tracks in the N/O–O/H plane and to check, with a wide grid of chemical evolution models, if the results are acceptable as compared with the observational data trends. In order to do this task, we need a large number of models with the same basic assumptions about the evolution and where only the star formation be varied. Therefore, we analyse the results obtained for the evolution of nitrogen with the wide grid of models shown in Mollá & Díaz (2005), which simulates 44 galaxies with different total masses and 10 possible star formation efficiencies. The chosen sets of yields used for these computations were those from WW for massive stars and those from GAV05 for LIM stars, which were already calibrated as explained above. An advantage of using these yields is that the primary N comes from LIM stars with which the effect of variable star formation is probably more evident.²

In Section 2, we analyse the N/O–O/H results obtained with simple chemical evolution models, by describing how elemental abundances of N and O evolve. In Section 3, we summarize the resulting abundances for the multiphase chemical evolution model with a primary nitrogen contribution coming from LIM stars variable with Z. Section 4 is devoted to the results obtained when the same code is applied to a wide grid of simulated galaxies with different masses and star formation efficiencies. Our conclusions are in Section 5.

2 THE CLOSED BOX MODEL PREDICTIONS

Nitrogen needs a seed of carbon or oxygen to be created from the CNO cycle. If this seed already exists when the star forms, N will be produced as a secondary element, which implies that its relative abundance N/C (or N/O) will increase proportionally to the original abundance of C or O. If the seed is created in the same star, just before N, then N is primary, and its abundance will be proportional to the C or O abundance, which means that N/C or N/O will maintain a constant value. Both trends are easily obtained using the classical and well-known CBM following which the abundance of an element i , Z_i , is related to the gas fraction, $\mu = g/M$, or ratio of the gas mass to the total mass in the region (Pagel et al. 1979; Tinsley 1980), through the expression: $Z_i = p_i \ln \mu^{-1}$, where p_i is the stellar

yield, the new production of an element i by a generation of stars. If nitrogen and oxygen are both primary, with yields $p_N = ppN$ and $p_O = pO$, respectively, then the relative abundance Z_N/Z_O is

$$\frac{Z_N}{Z_O} = \frac{ppN}{pO} = \text{constant}. \quad (1)$$

If, instead, nitrogen is secondary, its stellar yield $p_N = psN$ will depend on the abundance of the *seed*, in this case oxygen, and then $p_N = psN \times Z_O$ and, therefore,

$$\frac{Z_N}{Z_O} = \frac{psN}{2pO} Z_O. \quad (2)$$

Actually, the mechanism to form N in stars is mostly secondary, with a behaviour the same as the one shown by the line named NS in Fig. 1. However, the observed data (taken from references given in Table 1) indicate, as we may see in the same figure, that a primary contribution of N is necessary to explain the behaviour of data in the Universe. A line such as this one marked with NP shows the expected behaviour with a primary contribution plus a secondary one. This last one is only apparent when the oxygen abundance is high enough ($12 + \log(O/H) > 7.5-8$), marked as NP+NS. Obviously, if we change the yield ppN or psN , the lines would move towards higher or lower N/O abundances. The two lines shown in the figure have, in fact, been drawn to show the possible range of the data. It is clear that only a line cannot explain the observed dispersion but it is also evident that both components are necessary to obtain the trend shown by the data.

Nevertheless, a primary behaviour does not imply necessarily a constant value of N/O for the whole time-evolution, since we must take into account the mean-lifetimes of stars. The above results are obtained, as usual, with the classical hypotheses in the CBM that all stellar products are ejected simultaneously in the ISM. Some NP is easily produced by LIM stars in the range of $[4-8] M_\odot$ (Renzini & Voli 1981; van den Hoek & Groenewegen 1997; Marigo et al. 1998;

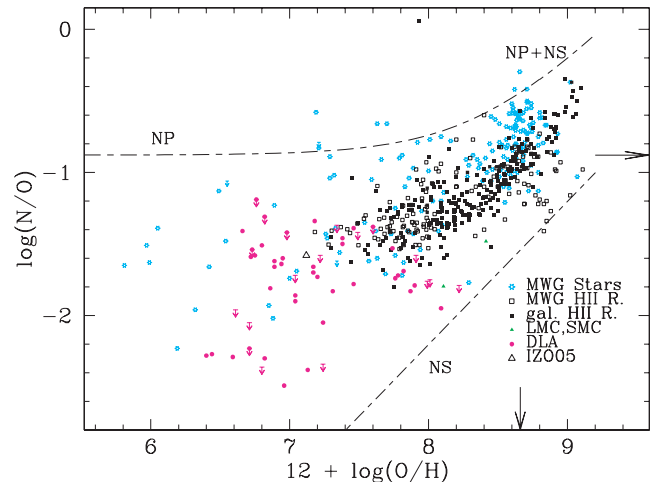


Figure 1. The relative abundance $\log(N/O)$ as a function of the oxygen abundance, $12 + \log(O/H)$, when N is secondary, shown by the line NS, and when primary, marked as NP, or a combination of both primary + secondary, marked as NP+NS. The points are the available data taken from the references of Table 1 for stars of our Galaxy, Galactic and external galaxy HII regions, Large Magellanic Cloud and Small Magellanic Cloud galaxies and DLA objects as labelled. The lowest-metallicity known galaxy (SBS0335–052) from Izotov, Thuan & Guseva (2005) is marked as the open triangle. The arrows mark the solar values in the graph and the short–long-dashed lines delimit the region occupied by the observational data.

² Since the objective of this work is to explore if different star formation efficiencies produce different tracks in the N/O–O/H plane, we must use the same ingredients for all our realizations, except the parameter we want to check. This is similar to the usually applied method when the stellar yields are the free parameters. In that case, using the same ingredients, except the stellar yields, for some GCE models, it is possible to determine what set of yields is the most adequate.

Table 1. References for N and O stellar abundances used for the comparison.

MWG Stars
Clegg, Tomkin & Lambert (1981)
Daflon & Cunha (2004)
Gratton et al. (2000)
Gummersbach et al. (1998)
Israelian et al. (2004)
Smartt et al. (2001)
Spite et al. (2005)
MWG H II Regions
Carigi et al. (2005)
Esteban et al. (1999a), Esteban, Peimbert & Torres-Peimbert (1999b), Esteban et al. (1999c)
Fich & Silkey (1991)
Peimbert (1979)
Shaver et al. (1983)
Tsamis et al. (2003)
Vilchez & Esteban (1996)
External galaxy H II regions
Garnett et al. (1995), Garnett et al. (1999)
Izotov & Thuan (1999)
Izotov et al. (2005)
Nava et al. (2006)
Tsamis et al. (2003)
van Zee et al. (1998), van Zee, Skillman & Haynes (2006)
van Zee & Haynes (2006)
DLA objects
Centurión et al. (2003)
Prochaska et al. (2002)
Pettini et al. (2002)

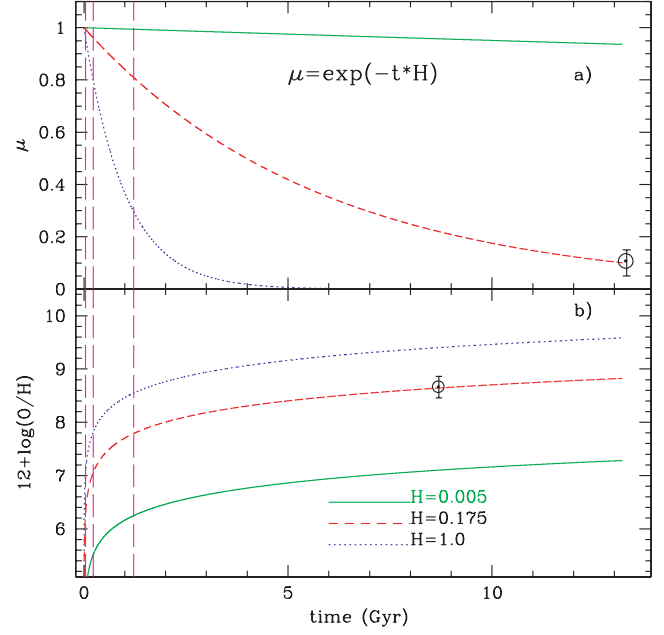
GAV05) during the HBB process. Since these stars died after the bulk of oxygen created by massive stars was ejected, if they are the main producers of the NP, this N would appear in the ISM later than the oxygen does. In this scheme, if the necessary NP was ejected by the LIM stars, one would expect that N/O will be flat only after the oxygen has already reached a certain level of abundance, giving time for nitrogen to appear, but it will not be constant before that moment.

In that case, the evolution of the N abundance is given by the following equation, taken from appendix B in HEN:

$$Z_N = \frac{ppN}{pO} \exp\left(\frac{Z_\tau}{pO}\right) (Z - Z_\tau) F + \frac{psNppC}{2pO^2} Z^2 + \frac{psNpsC}{6pO^2} Z^3, \quad (3)$$

where ppC and psC refer to the carbon primary and secondary yields, analogous to ppN and psN , and F is a step function that has a value of zero except if $Z > Z_\tau$. The abundance of N is, this way, computed as a function of the oxygen abundance, $Z = Z_O$, which will be ejected by short mean lifetime massive stars, that is, almost immediately after the formation of the first stars. The nitrogen has a secondary component that also appears in the ISM from early times (second and third terms), and another primary contribution, only produced by LIM stars, which will appear in the ISM with a certain delay (first term).

This delay translates into the fact that the NP will appear only when the oxygen abundance has already reached a certain value Z_τ ,

**Figure 2.** (a) The time-evolution of the fraction of gas $\mu = \exp(-tH)$ for three different values of $H = 0.005, 0.175$ and 1 , as given in the bottom panel; (b) the time-evolution of the oxygen abundance $12 + \log(O/H)$ for the same models as shown in (a). The long-dashed (magenta) lines mark the times $t = 0.040, 0.221$ and 1.21 Gyr. The solar region values are indicated in both panels.**Table 2.** Values of oxygen abundances Z_τ reached when LIM stars die for different values of the parameter H .

M_{star} (M_\odot)	H_1 (1.000)	H_2 (0.175)	H_3 (0.005)
2	0.399×10^{-2}	0.695×10^{-3}	0.200×10^{-4}
4	0.729×10^{-3}	0.131×10^{-3}	0.376×10^{-5}
8	0.123×10^{-3}	0.229×10^{-4}	0.660×10^{-6}

reached in the time when the LIM stars died. Actually, the LIM stars do not have large mean-lifetimes τ . Using the age–stellar mass relation obtained by the Geneva group isochrones (Schaller et al. 1992), stars of 2, 4 and 8 M_\odot have mean lifetimes of $\tau \sim 1.21, 0.228$ and 0.040 Gyr, respectively, short in chemical evolution terms. In order to calculate the abundances Z_τ , reached when these stars die, we use again the CBM: $Z_\tau = p \ln \mu^{-1} (t = \tau)$. For computing the values of the gas fraction at those times we assume that it is a decreasing exponential function of time: $\mu(t) = \exp(-tH)$, where H is the efficiency to form stars (equal to the inverse of the time-scale for consuming the gas, $1/\tau_{\text{gc}}$). We show in Fig. 2(a) the time-evolution of this function $\mu(t)$ for three different values of $H = 0.005, 0.175$ and 1.0 (or $\tau_{\text{gc}} = 200, 5.75$ and 1 Gyr). In panel (b), we show the time-evolution of the oxygen abundance, as $12 + \log(O/H)$, corresponding to each one of these parameters H . We give in Table 2 the values of Z_τ reached in these closed models when $t = \tau$ for stars of 2, 4 and 8 M_\odot computed using $pO = 3.3 \times 10^{-3}$, $ppC = 1.2 \times 10^{-3}$, $psC = 0.9$, $ppN = 2.2 \times 10^{-4}$ and $psN = 0.130$ as stellar yields for oxygen, the primary and secondary carbon, and the primary and secondary nitrogen, respectively.

In Fig. 3(a), we show how the N/O evolves when O/H increases in the model corresponding to $H = 0.175$ for the three

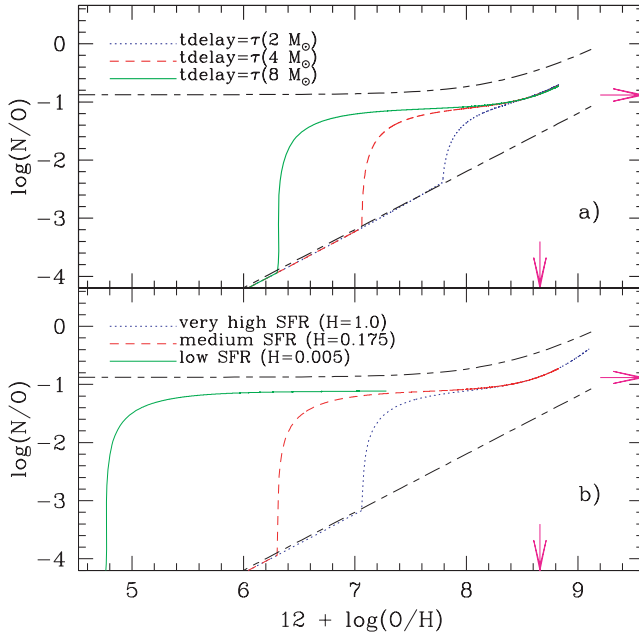


Figure 3. The relation of $\log(N/O)$ with the oxygen abundance, $12 + \log(O/H)$, by assuming that the gas fraction is an exponential decreasing function of time, obtained by equation (4) with two contributions. The primary component appears in the ISM: (a) when stars of 2, 4 and $8 M_{\odot}$ die, the dotted, short-dashed and solid lines, respectively, with a parameter $H = 0.175$; (b) when stars of $8 M_{\odot}$ die by assuming different values for H as marked in the figure. The short-long-dashed lines and the arrows have the same meaning as in Fig. 1.

possible values of column 3 of Table 2, which would be the oxygen abundance reached by assuming an NP coming from stars of 2, 4 and $8 M_{\odot}$. We may distinguish the following three phases in that figure.

(i) The N/O increases smoothly as secondary from the first phases of the evolution, for $Z < Z_{\tau}$, with a clear slope that corresponds to the secondary contribution of massive stars.

(ii) The NP appears in the ISM when $Z = Z_{\tau}$, increasing very rapidly the relative abundance (N/O). The final value of this phase is given by ppN/pO . This feature must not be erroneously taken as a secondary behaviour.

(iii) After this exponential function, the secondary behaviour coming from LIM stars³ appears again.

The following two evident facts appear in that graph.

(i) The change from the NS to the NP regime occurs very abruptly.

(ii) The oxygen abundance at which this change occurs is very dependent on the SFR and on the mass of the first stars ejecting NP.

Obviously, if NP were ejected by stars of $2 M_{\odot}$, which is not a realistic case, there would be more time for oxygen abundances to increase, and so the value Z_{τ} would be higher than that in the case of NP ejected by stars of $8 M_{\odot}$. In the last case ($8 M_{\odot}$), the abrupt increase of N/O appears at the left-hand side in the figure N/O–O/H, whereas the first one ($2 M_{\odot}$) produces this increase at the right-hand side of the figure. The higher the mass of the stars

ejecting NP, the lower the oxygen abundance for which the change takes place.

On the other hand, it is also evident that these Z_{τ} abundances, shown in Table 2, depend on the SFR: in Fig. 3(b), we show the results obtained using the values Z_{τ} shown in the last line of Table 2, assuming that stars of $8 M_{\odot}$ are responsible for producing NP. If the SFR is strong ($H = 1.0$, solid line), the oxygen abundance increases very rapidly, so when the NP begins to be ejected, O/H has already reached a high value. In contrast, if the SFR is low ($H = 0.005$, dotted line), oxygen maintains a low abundance for a long time. It is therefore possible that nitrogen will be ejected when O/H is still below $12 + \log(O/H) < 7$.

The CBM provides approximated results, even for oxygen abundances, since it is valid only if $Z \ll 1$ which is no longer valid when the fraction of gas is small. Furthermore, the hypothesis of a gas fraction decreasing with time is not valid for a disc which forms from the gas infalling from the halo. In fact, the evolution of the gas fraction predicted by a CBM with $H = 0.175$, which might represent the solar vicinity, is very similar to the one obtained with a numerical model by GAV05 for the solar region. Both models differ, however, at the earliest phases: first, the numerical model maintains a higher value than that maintained by the equivalent CBM, and then it rests below this last one. Finally, both reach a similar value of ~ 0.10 as observed. The oxygen abundances are not equivalent, either, to the CBM ones. The GAV05 model needs more time to reach an oxygen abundance $12 + \log(O/H) = 7$. This occurs just when the first LIM stars begin to die, so it is important to bear in mind that, in a realistic case, when LIM stars begin to die, the oxygen abundance may be even lower than that predicted by a CBM model.

In summary, the stellar yields and the mass range of stars (or their mean-lifetimes) that produce nitrogen are important to determine the possible evolution of N/O versus O/H, but the star formation history is also essential to determine the track followed by a given region or galaxy in the plane N/O–O/H.

3 THE MULTIPHASE CHEMICAL EVOLUTION MODEL

3.1 Abundance calculations

Now we use a numerical code which takes into account the stellar mean-lifetimes and other more realistic assumptions for the scenario and input prescriptions (infall rate, masses, geometry, etc.). The next calculations have been performed with the multiphase model, a numerical code developed by Ferrini et al. (1992), and widely described in that work and in the following ones (Ferrini et al. 1994; Mollá, Ferrini & Díaz 1996) of the same group.

As is explained in Ferrini et al. (1992), the equation to compute the abundances of each element i in the gas, X_i , is:

$$\frac{dX_{iG}d}{dt} = -X_i\Psi + X_{i,H}fg_H + W_i(t), \quad (4)$$

where W_i is the ejected mass rate (*new + old*) for each element i by the stars, g_D the gas mass, Ψ the SFR in the modelled disc region and fg_H the infall rate, assuming as usual that there exists a gas *infall* from the halo to the disc. The ejected metal mass rates or restitution rates $W_i(t)$ are computed following the formalism of **Q** matrices, well described in the cited work (Ferrini et al. 1992) and also in other works, such as Portinari, Chiosi & Bressan (1998). We recommend these works to the reader for a clear explanation of equations.

³ We have used the same psN for both massive and LIM stars, although it may have a different value for each mass range.

The expression to compute the term W_i is

$$W_i(t) = \int_{m, \tau=t}^{m_{\text{up}}} \sum_j \tilde{Q}_{i,j}(m) X_j(t - \tau(m)) \Psi(t - \tau(m)) dm, \quad (5)$$

where m_{up} is the upper limit of the initial mass function $\Phi(m)$, the expression $\tilde{Q}_{i,j} = Q_{i,j} \Phi(m)$ represents the matrix $Q_{i,j}$ multiplied by the initial mass function $\Phi(m)$, and $Q_{i,j}$ are defined as

$$Q_{i,j}(m) = \frac{\text{mexp}_{i,j}}{m_j} = \frac{\text{mexp}_{i,j}}{m X_j}, \quad (6)$$

where $\text{mexp}_{i,j}$ is the ejected mass of each element i which was originally in the star as element j . This way, the total fraction of element i ejected by each type of stars with mass m is

$$\frac{\text{mexp}_i(m)}{m} \Phi(m) = \sum_j \frac{\text{mexp}_{i,j}}{m} \Phi(m) = \sum_j \tilde{Q}_{i,j}(m) X_j. \quad (7)$$

When there are two components, primary and secondary, for an element, as occurs with N, it is necessary to know both contributions for each star and to compute them separately in the model. The multiphase model uses for that the equations shown in Ferrini et al. (1992), similar to those shown by Portinari et al. (1998) in their appendix B.

3.2 Parametric study

The above cited expressions are those included in the multiphase chemical evolution code from Ferrini et al. (1992, 1994) where yields from Renzini & Voli (1981) for LIM stars and from Woosley & Weaver (1986) for massive stars were used to model the GCE. Taking into account our previous findings, it is evident that not only do the stellar yields play a role in the resulting evolution of N in a region or galaxy, but also the star formation history is very important in determining the track followed by a given object in the plane N/O–O/H. A distinct feature is shown in this plane when

the NP is ejected to the ISM, and this feature appears at higher or lower oxygen abundances depending on the SFR: the stronger the SFR, the higher the oxygen abundance at which this characteristic increase appears. Therefore, it is necessary to analyse how N evolves when different input parameters, related to the SFR, are chosen for a given multiphase chemical evolution model such as this one used in Ferrini et al. (1994).

We therefore analyse in detail this influence of these input parameters (see Mollá & Díaz 2005, for a wide explanation of the multiphase model and its parameters) over the N/O evolution. For that, we have computed some family of generic models (that is, they are not models applicable to MWG), all of them using only a matrix \mathbf{Q} corresponding to one metallicity.

(i) Three models where the SFR in the halo, represented by its efficiency ϵ_K , takes three different values: $\epsilon_K = 0$, $\epsilon_{K,\text{std}}$, and $100 \times \epsilon_{K,\text{std}}$, where $\epsilon_{K,\text{std}}$ is the value used in Ferrini et al. (1994), and subsequent multiphase models, for the MWG halo.

(ii) Three models where there is no star formation in the halo, $\epsilon_K = 0$, and where only the density of the initial mass gas changes from one model to the next.

(iii) Three models where there is no star formation in the halo, $\epsilon_K = 0$, and where efficiencies to form stars are the same, but with a total mass and an infall rate different for each model.

(iv) Three models where there is no star formation in the halo, $\epsilon_K = 0$, and where the total mass and the infall rate are the same for all models, but where efficiencies to form stars are different for each one.

The results of these models are shown in Fig. 4. In each panel, we show the variations in the N/O track by the change of one parameter as described. It is clear from these results that there are some parameters which may change the N evolution since the early phases of the evolution. Only in panel (b) does N/O show a similar evolution for all densities. Instead, the evolution of N/O depends

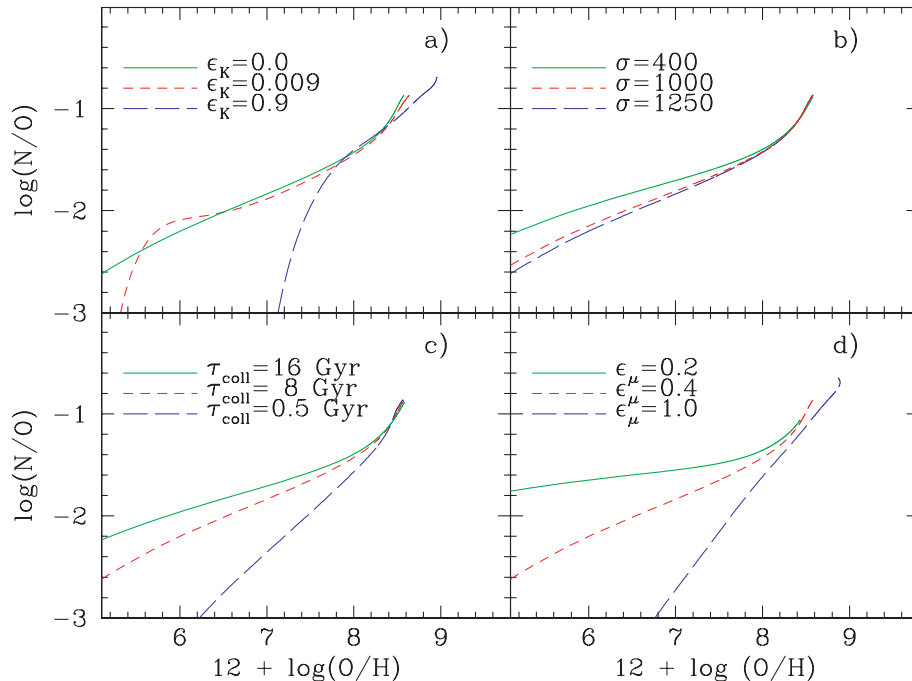


Figure 4. The effect of varying the input parameters of some generic chemical evolution models on the evolution of the relative abundance $\log(\text{N}/\text{O})$ versus the oxygen abundance $12 + \log(\text{O}/\text{H})$: (a) the effect of the star formation of the halo; (b) the effect of the different initial density of gas mass in the region; (c) the effect of the infall gas rate; and (d) the effect of the star formation efficiencies.

very strongly on the SFR (either in the halo or in the disc). The effect of the halo star formation is only evident if ϵ_K is sufficiently high. If it is low enough, the variations for $12 + \log(\text{O}/\text{H}) > 6$ are indistinguishable in the resulting track.

As before, the N/O evolution shows a flatter or a steeper behaviour depending on the type of scenario or model defined by the parameters of star formation in the halo, the possible infall rate from the halo to the disc, and the SFR in the disc. We recall that a strong star formation in the halo in the earliest phases of the evolution, before stars form in the disc, as it is thought occurred in our Galaxy, produces a shift of the N/O track in the plane N/O–O/H towards high oxygen values and a slope similar to this shown in Fig. 3 for the model in which the NP is ejected by the lowest-mass stars. On the other hand, if there is no star formation in the halo, as occurs in the three other panels, or it is low enough, the abrupt *change of phase* disappears in our graphs, just because it occurs at lower oxygen abundances than those shown in the figure. This way the track simulates a smoother behaviour. Therefore, variations of input parameters and scenarios may explain, at least partially, the differences found when chemical evolution models in the literature, using the same set of yields, are compared.

The old version of the Galactic multiphase chemical evolution model from Ferrini et al. (1992, 1994) was computed with the same efficiency to form stars and molecular clouds for all MWG disc regions. It, however, uses collapse time-scales and total masses variable with the galactocentric radius of each radial region. Furthermore, it is necessary to take into account that there exist differences in the geometry of each region. All of these variations produce different radial densities. And, hence, the resulting star formation histories show higher and earlier maximum values at the inner regions of the disc than at the outer ones. Thus, different radial regions of the disc show a behaviour in agreement with the previous section: a more *secondary* track for the strong star formation regions of the inner disc, and less steep for the outer region ones in which the star formation was smoother.

3.3 The effect of the metallicity-dependent yields

The stellar models and their corresponding yields of elements depend now on metallicity and, therefore, a set of matrices (**Q**) for each metallicity is used.⁴

We have computed a GCE model, following the same prescriptions given in Ferrini et al. (1994) and Portinari et al. (1998) but using the metallicity-dependent yields from van den Hoek & Groenewegen (1997) for LIM stars and from WW for massive stars. The resulting model reproduces well the star formation history and the age–metallicity relation for the solar vicinity, as is shown in GAV06. The radial distributions of diffuse and molecular gas, SFR and oxygen abundance also fit the observational constraints.

⁴ Like Ferrini et al. (1992), Portinari et al. (1998) claimed that the $Q_{i,j}$ formalism has some advantages since it compensates for the lack of metallicity-dependent yields. One may think that the use of matrices **Q** may be avoided when these kinds of yields are already available. However, as Portinari et al. (1998) explained: ‘stellar models with different metallicities generally assume solar relative abundances of the various species within a given Z ; but abundance ratios are not constant in the course of galactic evolution, nor they are in the evolution of a chemical model. The ... matrix links any ejected species to all its different nucleosynthetic sources, allowing the model to scale the ejecta with respect to the detailed initial composition of the star through the ...’ (matrices **Q**). Therefore, like these authors, we continue using the same formalism.

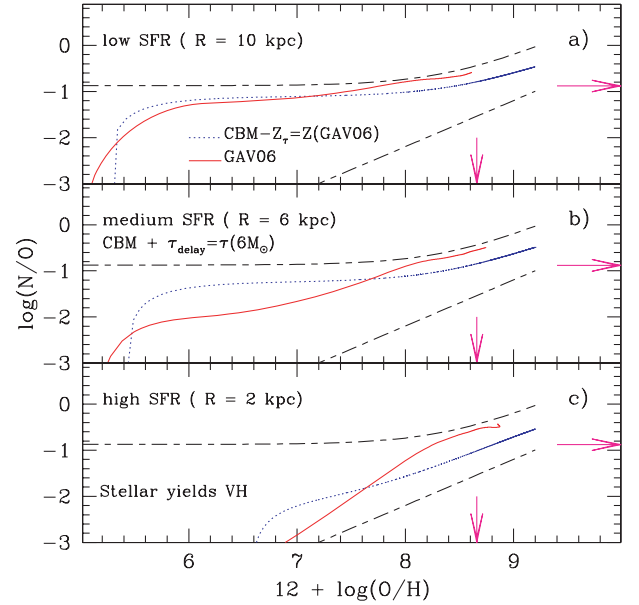


Figure 5. The relation N/O–O/H obtained using the stellar yields for LIM stars from van den Hoek & Groenewegen (1997, VH), with the Galactic multiphase chemical evolution model from GAV06, for three regions of the Galactic disc located at (a) 10, (b) 6 and (c) 2 kpc galactocentric radius, the solid (red) lines. Each line is compared with the CBM results (dotted lines) computed assuming a delay $Z_\tau = Z(t = \tau(6 M_\odot))$ taken from the corresponding region multiphase model, and using equations (8) and (9) as the metallicity-dependent yields ppN and psN . The short–long-dashed lines and the arrows have the same meaning as in Fig. 3.

In Fig. 5, we represent the evolution of $\log(\text{N}/\text{O})$ versus $12 + \log(\text{O}/\text{H})$ for this model. In each panel, we compare the results for an outer, medium and inner Galactic disc region, as labelled in the figure (solid line), with CBM models (dotted lines) computed assuming that NP appears when stars of $6 M_\odot$ die. The values for the abundance Z_τ , shown in Table 3, are taken from the same multiphase models for $t = \tau(6 M_\odot)$.⁵ In this case, we have used the set with $\eta_{\text{AGB}} = 4$ and $m_{\text{HBB}} = 0.8 M_\odot$ of metallicity-dependent yields from van den Hoek & Groenewegen (1997), which have been included in the CBM, after a fit with least-squares functions, by the expressions

$$ppN = 1.0 \times 10^{-8} z_\tau^{-0.76}, \quad (8)$$

and

$$psN = 0.29 + 1598 z_\tau. \quad (9)$$

This way, the values for the yields ppN and psN vary according to the abundance reached in the ISM when stars form.⁶ For a CBM all stars form simultaneously, so we have taken for this metallicity the value Z_τ . The resulting yields are given in the two last

⁵ Actually, in the multiphase models the maximum star formation moves towards later times for the outer regions compared with the early times in which the maximum occurs for the inner regions. Therefore, the Z_τ might be chosen taking into account this shift in the time-scale with respect to the zero time with which we have selected the values of Table 3.

⁶ This method is, in fact, an approximation: if ppN and psN depend on Z , it is necessary to perform a new integration and the final result is not equal to equation (3). We have checked that this approximation, easier to understand and to use, is good enough, giving a similar behaviour to the one obtained with the exact solution.

Table 3. Values of oxygen abundances Z_{τ} reached when LIM stars of $6 M_{\odot}$ died in the multiphase models VH from GAV06 and the corresponding values for ppN and psN .

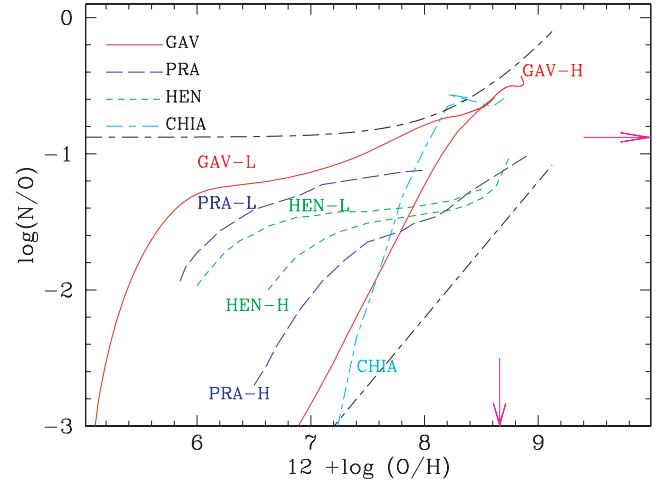
Radius (kpc)	Z_{τ}	OH_{τ}	ppN	psN
2	4.7×10^{-5}	6.60	2.01×10^{-5}	0.365
6	3.0×10^{-6}	5.40	1.66×10^{-4}	0.295
8	2.4×10^{-6}	5.30	1.99×10^{-4}	0.293
10	2.0×10^{-6}	5.24	2.23×10^{-4}	0.292
18	1.5×10^{-6}	5.10	2.83×10^{-4}	0.291

columns of Table 3. For high-metallicity regions, as the inner disc is located at 2 kpc, Z_{τ} is higher than that for a medium star formation region, such as the solar vicinity, and therefore ppN is lower, and $Z_N/Z_O = ppN/p$ will be also lower. This means that the saturation level of the exponential function given by equation (3) takes a value smaller than the one shown in Fig. 3. On the other hand, the value psN will be higher for the inner region than for the solar vicinity, and, consequently, the secondary behaviour due to LIM stars is stronger and more evident for the region at 2 kpc than for the one located at 6 or 10 kpc.

The same behaviour is apparent for the multiphase models. Thus, as is evident in that figure, the metallicity-dependent yields change the expected tracks in the plane N/O – O/H due to variations in the SFR, increasing the existing difference among them, especially if this SFR is strong enough. When it is very low, as occurs in panel (a), models give results similar to the ones corresponding to Fig. 3. When these metallicity-dependent yields are included in a model with strong star formation (panel c), the evolution changes appreciably compared with the equivalent track obtained with only one set of yields. This is reasonable: while Z is low, the model is similar to the one obtained with Q matrices computed with yields for only one metallicity. When the oxygen abundances increase, the stellar production is computed using other sets of yields. In particular, the yield of N increases, but the contribution of NS is relatively higher than before and the NP, which gives the final flat level of N/O , is smaller. This way, the evolution of N/O in a strong star formation model behaves more like secondary and the exponential shape seems smoother.

3.4 Comparison with other works

From the previous section, we have found that the track in the plane N/O – O/H is flat when the star formation is low and steep in the case of strong star formation. This effect is not new since, as we have already mentioned, some other works, such as Mouhcine & Contini (2002) and Lanfranchi & Friaça (2003), have found a similar behaviour, a flattening of the track in the N/O – O/H plot, when the star formation efficiency decreases. As an example, we compare in Fig. 6 our results with those obtained by other authors. All of them were computed using the same set of yields from WW for massive stars, and from van den Hoek & Groenewegen (1997) for LIM stars. Our Galactic models for radial regions located at galactocentric radii $R = 2$ and 10 kpc are represented by the solid line. Since each radial region has its own total mass, gas infall rate, efficiencies, and volume, the star formation history results are different for each one, slow and low in the outer region, and strong and early in the inner one. Correspondingly, they are marked as GAV-L and GAV-H, respectively. Other lines represent models from HEN, PRA and Chiappini, Matteucci & Meynet (2003, hereafter CHIA), marked in

**Figure 6.** The evolution of the relative abundance, $\log(N/O)$, with the oxygen evolution, $12 + \log(O/H)$, for two multiphase chemical evolution models – GAV, computed using the yields from van den Hoek & Groenewegen (1997) and WW and the mean-lifetimes from Schaller et al. (1992), compared with those obtained in models from HEN, PRAN and CHIA. The line coding is given in the figure. Each model, except CHIA, is marked as L or H denoting that the SFR is low or high. The short–long-dashed lines and the arrows have the same meaning as in previous figures.

the plot. The first two authors give two models with high (represented with an H) and low (represented with an L) star formation efficiency. Both authors obtained tracks that are rather flat in the plane N/O – O/H when the star formation is low, with a change of phase at $12 + \log(O/H) \sim 6$ – 6.3 , while the strong star formation model shows this feature at $12 + \log(O/H) \sim 7$. CHIA's model shows a steeper behaviour more according to our model for strong star formation (probably due to their strong star formation in the halo).

It is evident that our models behave similarly to others in the variation of N/O tracks with the usual input parameters of chemical evolution models. We claim that a flat behaviour for the evolution of N/O versus O/H is a usual characteristic of regions or galaxies where the star formation occurs quietly maintaining a low value for a long time. The presence of this flat behaviour in the N/O – O/H plot is not only due to the used yields.

Since the effect of the star formation is important, it also appears using any other yield set with NP ejected by LIM stars. Obviously, the absolute values of the ratio N/O depend on the yield set used. GAV05 presented a set of LIM star yields which are very similar to those calculated by Dray et al. (2003) from accurate stellar models – see fig. 5 in GAV06 – but span a wider range in mass and metallicity as required in chemical evolution models. They were computed with a similar technique to that used by van den Hoek & Groenewegen (1997) but with updated inputs. The main difference between these two sets of yields resided in the contribution of the primary (or secondary) component to the total nitrogen yield by LIM stars, which is larger in GAV05 by factors of between 2 and 4 depending on metallicities, even though the total N integrated yield is larger in van den Hoek & Groenewegen (1997) at all metallicities (see fig. 3 from GAV06). These yields were included and successfully calibrated in a GCE model in GAV05 and GAV06, reproducing the classical observational constraints (star formation history, radial distributions of gas, etc.) and obtaining N abundances in agreement with the MWG stellar data. In particular, the flat behaviour shown by the metal-poor star data of the Galactic halo is very well reproduced (see fig. 12 in GAV06).

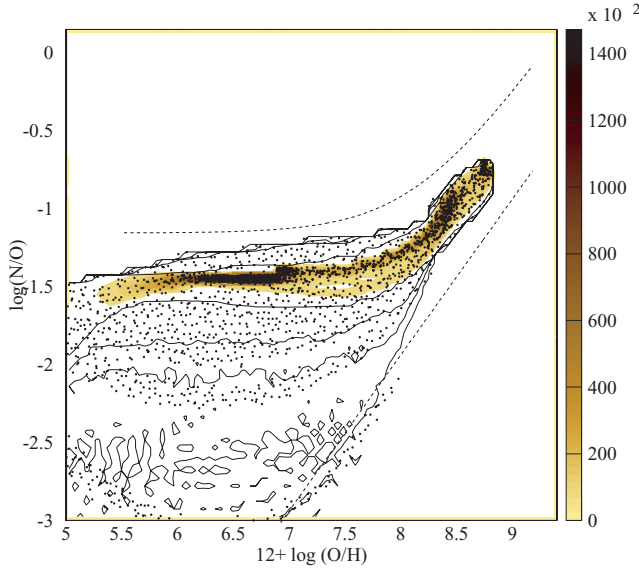


Figure 7. The relation between N/O and O/H for the simulated galaxies. The complete results for all modelled regions are shown as the small dots. The coloured contours represent the isolines of number of points included within them (see relative scale to the right), while the solid lines represent the regions with 0.3, 0.03, 0.012 and 0.003 per cent, respectively, of the total number of points. The data region is delimited by the two dashed lines.

4 THE GRID RESULTS: N/O VERSUS O/H FOR SPIRAL AND IRREGULAR GALAXIES

The grid of chemical evolution models from Mollá & Díaz (2005)⁷ was parametrized by the initial mass radial distribution. For each one of our 44 theoretical galaxies, defined by this mass distribution, 10 different sets of efficiencies of molecular cloud formation and star formation were used, providing 10 evolutionary tracks. Thus, a total of 440 models were computed. For each one, a set of radial regions, variable according to the size of the theoretical galaxy, were modelled. Therefore, a large number of possible evolutionary tracks are finally available to compare with observations. The massive star yields from WW and the above cited new yields for LIM stars from GAV05 have been used for calculating this grid of models. Even though there are still some uncertainties in the AGB phase treatment and in the quantity of the NP that LIM stars may create, we consider that the set of stellar yields from GAV05 has been well calibrated and, therefore, that it is adequate to our purposes.

We ran models that represent the evolution of different regions of galaxies, assuming that there is also star formation in the halo (with a constant efficiency for all models), and that infall rates, initial masses of gas and efficiencies to form stars are all different from one modelled galaxy to the next. All these factors multiply their effects, changing the resulting star formation history. Thus, the final results show very different evolutions of the N/O versus O/H as we will show in the following figures.

In Fig. 7, we show the results for the relative abundance $\log(N/O)$ versus the oxygen abundance, $12 + \log(O/H)$, obtained with an updated grid of models, computed with the same inputs and hypotheses as those of Mollá & Díaz (2005) but using as stellar mean-lifetimes those computed from Schaller et al. (1992), instead of those from

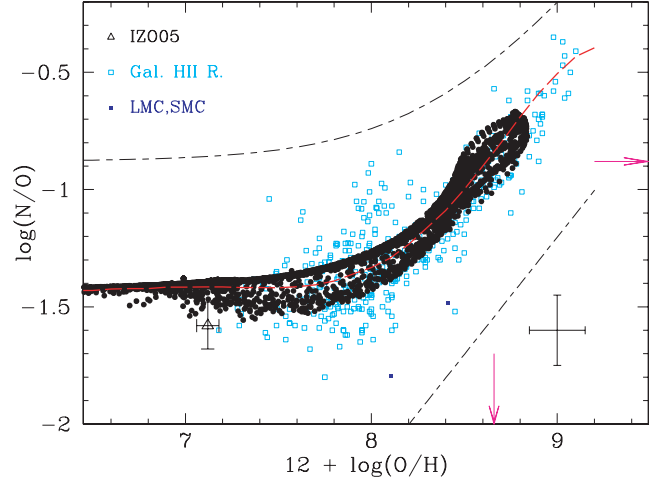


Figure 8. The relative abundance, $\log(N/O)$, versus the oxygen abundance, $12 + \log(O/H)$, for the present time as full (black) dots compared with the data corresponding to Galactic and extragalactic H II regions, represented as open (cyan) squares. The long-dashed (red) line is the least-squares fitting function. The large open triangle around $12 + \log(O/H) \sim 7.1$ is the value found by Izotov et al. (2005) for the lowest-metallicity star-forming galaxy known. The short-long-dashed lines and the arrows have the same meaning as in Fig. 3.

Burkert & Hensler (1987) used in our previous version. There we show the whole set of results,⁸ for all calculated times⁹ and models, as small dots. Over them we have plotted some contours in yellow levels, defined by the scale located to the right-hand side. Furthermore, we draw some other contours as solid lines for regions with 0.3, 0.03, 0.012 and 0.003 per cent, respectively, of the total number of points.

It is evident that the generic trend obtained with our models using the new yield set looks very similar to that shown by the data which lie in the region defined by the dashed lines. The predicted dispersion is also large, as shown by the observations.

In Fig. 8, we only represent the present-time results, as full points, that we compared with the Galactic and extragalactic H II region data, as the open squares, taken from references given in Table 1. Our models may be fitted by a least-squares polynomial function, shown by the long-dashed line in the same plot:

$$\log(N/O) = -1149.31 + 1115.23x - 438.87x^2 + 90.05x^3 - 10.20x^4 + 0.61x^5 - 0.015x^6,$$

where $x = 12 + \log(O/H)$.

It is evident that our models reproduce adequately the trend of present-day data, and even a certain dispersion. There are two zones where data fall out of the model region. The first one corresponds to the high-metallicity H II ($Z > Z_{\odot}$) regions, where it is difficult to estimate directly elemental abundances. In fact, recent estimations for some of this kind of region seem to produce lower oxygen abundances than the old ones, estimated through other empirical methods (Castellanos, Díaz & Terlevich 2002; Pilyugin 2004). Therefore, it is probable that those points must be corrected. The second region corresponds to oxygen abundances around $12 + \log(O/H) = 8$,

⁷ See this work for details about the chemical evolution models, available at <http://vizier.u-strasbg.fr/viz-bin/VizieR?-source=J/MNRAS/358/521>.

⁸ These updated results are available in electronic format at <http://wwwae.ciemat.es/~mercedes/grid.chemev.html>.

⁹ The time-step used for writing results is 0.1 Gyr. Obviously, if we plot results with a smaller time-step, the graph will be more densely populated.

just when the parameter R_{23} , usually used to estimate O/H in the low-metallicity regions, is two-valued, thus increasing the data errors above the usual error bar (shown in the plot). On the other hand, it is well known that some nearby star-forming galaxies show evidence of galactic winds and there are a large number of works (Hensler, Theis & Gallagher 2004; Marcolini, Brighenti & D’Ercole 2004; Recchi et al. 2006; Recchi & Hensler 2006; Romano, Tosi & Matteucci 2006) including this possibility in their evolution models. We cannot discard the existence of outflows in the galaxies whose data our models do not reproduce and, maybe, this is the solution of this disagreement. However, in general, these winds are important only in young ($< 10^7$ yr) starbursts that form many massive stars in a metal-rich environment ($Z > Z_{\odot}$) (Veilleux, Cecil & Bland-Hawthorn 2005). Recent X-ray observations (Rasmussen, Stevens & Ponman 2004; Grimes et al. 2005; Ott, Walter & Brinks 2005) show evidence of these winds in dwarf galaxies, but only for those suffering a starburst, which means $\text{SFR} > 5 M_{\odot} \text{yr}^{-1}$. This high SFR is not always present in dwarf galaxies. On the other hand, the dwarf irregular galaxies with rotation velocity higher than 30 km s^{-1} seem to be able to retain their gas-rich discs (Garnett 2002; Dekel & Woo 2003). Thus, the discussion of this subject requires a study of individual galaxies which fall out of the scope of this work and which we hope to treat in the near future. In any case, the least-squares fitting function, also represented in the figure, has a behaviour in agreement with the generic trend of data, even at the high-abundance end.

In order to see the effects of the galaxy total mass and/or the variations of the star formation efficiencies on the computed abundances, we show in Fig. 9 the evolutionary tracks of N/O abundances for two limiting models: (1) that corresponding to the most-massive galaxy with the highest molecular cloud and star formation efficiencies – model M, solid lines, and (2) that corresponding to the least-massive galaxy and with the smallest efficiencies – model L, dotted lines. Each line represents various radial regions in the same time-step, given in the plot in Gyr. We would like to stress that these lines are

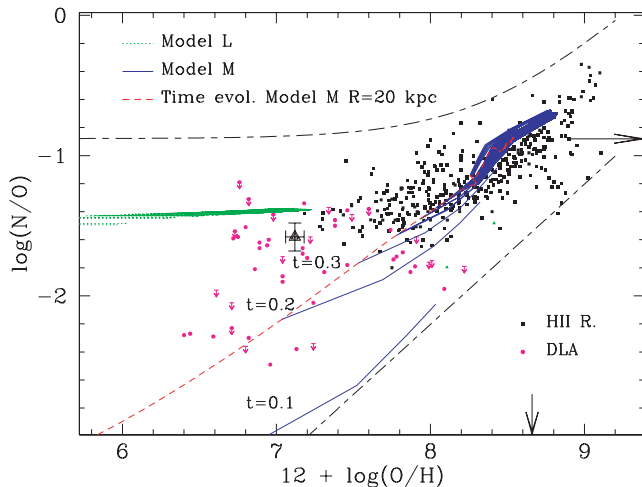


Figure 9. The relation between N/O and O/H for the most-evolved and most-massive galaxy, model M, solid (blue) lines, and for the lowest-mass and least-evolved galaxy, model L, dotted (green) lines, while the short-dashed (red) line indicates the time-evolution of a region at 20 kpc of galactocentric distance of model M. The small full squares are the H II region data, while the full triangle (magenta) dots are the DLA object data. The large triangle around $12 + \log(\text{O}/\text{H}) \sim 7.1$ is the value found by Izotov et al. (2005) for the lowest-metallicity star-forming galaxy known. The short-long-dashed lines and the arrows have the same meaning as in Fig. 3.

not evolutionary tracks in time. To obtain those, it is necessary to join the points corresponding to a given radial region of a galaxy at different time-steps as we have done with the short-dashed line. It is clear from this plot that the exact mode in which the star formation takes place determines the evolution of the N/O ratio. In the first type of galaxy, there is an intense star formation episode, occurring early in time and declining afterwards, simulating an early morphological type bright galaxy. The second example shows a low and continuous SFR producing an object similar to a dwarf galaxy. In the first case, N/O evolves very quickly showing a secondary trend, beginning from $\log(\text{N}/\text{O}) \sim -2.5$ dex when the oxygen abundance is already $12 + \log(\text{O}/\text{H}) \sim 7$ dex, while in the second case, N/O keeps a very constant value of $\log(\text{N}/\text{O}) \sim -1.4$ dex along the whole evolution, with oxygen abundances $12 + \log(\text{O}/\text{H}) \leq 7$. These two models define a region similar to the one predicted by Vila Costas & Edmunds (1993, see their fig. A1), but for the opposite reason: the less-evolved models have higher N/O ratios than the ones with strong SFRs and smaller time delays have.

Thus, the abundances shown by some metal-poor dwarf galaxies can be reproduced by models with a continuous SFR with low efficiencies. This is so, even taking into account the lifetimes of the LIM. In fact a delay in the ejection of N does not necessarily imply a low value of N/O. On the one hand, the time required to reach the N/O value shown by those galaxies ($\log \text{N}/\text{O} \simeq -1.5$) might be as short as $\sim 300\text{--}400$ Myr, because the intermediate-mass stars of $4\text{--}8 M_{\odot}$ (which contribute to the NP) have mean-lifetimes in the range $50 \leq \tau \leq 200$ Myr. On the other hand, and more importantly, low oxygen abundances do not necessarily imply a short evolution and a low enough star formation rate can keep abundances low during a long period of time.

These results are only partially due to the dependence on metallicity of the yields we use. The integrated ratio of the primary to total N yields $^{14}\text{N}_p/^{14}\text{N}$ (see fig. 3 in GAV06) has a value ~ 0.20 for Z_{\odot} (slightly smaller than the one estimated, approximately one-third, by Alloin et al. 1979, as necessary to reproduce the data) and it increases up to 0.6 for low metallicities. This contribution of NP, larger for low-metallicity stars than for high-metallicity ones, is important since it allows us to obtain tracks in the plane N/O–O/H flatter than the ones predicted with a constant contribution of the NP. We must make it clear, however, that if we eliminate the metallicity dependence from the yields, we still obtain different tracks for regions with different star formation histories, as we have shown in previous sections. Thus, the selection of the set of yields is not essential to obtain these differences among tracks, although the effect shown increases when metallicity-dependent yields are included in the models. Furthermore, the absolute level of observations and the fine tuning of the observed shape in the plane N/O–O/H for the present-time data are only reproduced if the stellar yields, in turn, give the right level of NP and have an adequate dependence on metallicity. The chemical evolution models must also be well calibrated in order to predict star formation histories able to produce abundances in agreement with data. Therefore, the adequate selection of metallicity-dependent LIM star yields, such as those from GAV05, combined with the use of accurate chemical evolution models, such as those from Mollá & Díaz (2005), allows us to obtain abundances for N and O which reproduce the complete set of data in the plane N/O–O/H.

Finally, in order to explore the time-evolution of the modelled abundances, we show in Fig. 10 the results for four different time-steps: $t = 0.1, 0.17, 0.30$ and 13.2 Gyr. These epochs would correspond to redshifts $z \sim 3.8, 3.7, 3.5$ and 0 , respectively, for a cosmology with $H_0 = 71 \text{ km s}^{-1} \text{ Mpc}^{-1}$, $\Omega_M = 0.30$, $\Omega_{\Lambda} = 0.70$, if

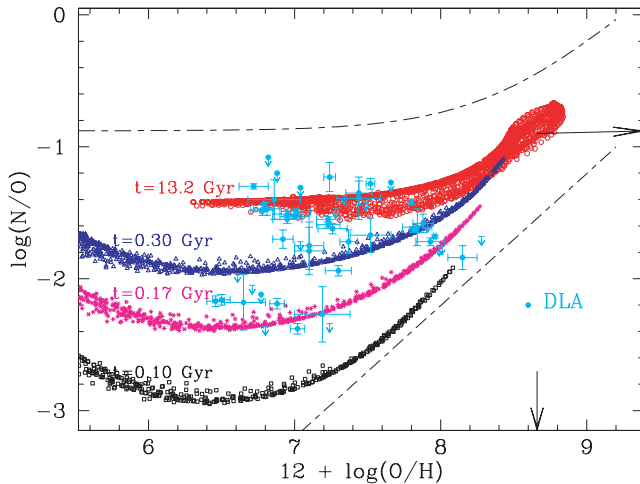


Figure 10. The relation N/O–O/H for different evolutionary times as marked in the figure. The full (cyan) dots correspond to DLA objects.

the formation of these spiral and irregular galaxies occurred at a redshift $z \sim 4$. A large gap appears between the results for each one of our time-steps. In particular, our models predict a feature similar to the so-called *second plateau* that Centuri n et al. (2003) claimed to exist at a metallicity around $12 + \log(\text{O}/\text{H}) \sim 7$, which appears at a level of $\log(\text{N}/\text{O}) \sim -2.3$ for $12 + \log(\text{O}/\text{H}) \sim 6.5\text{--}7$, while most points appear at a higher level of N/O (≥ -1.8) for a similarly low O/H abundance. In fact, no gap is apparent between models at 1.1 and 13.2 Gyr, thus making it difficult to discriminate objects at a redshift up to $z < 2.5$ from those at redshift $z = 0$ in the N/O–O/H plane, as is actually the case. The abundances predicted for galaxies at redshift $z \geq 3$ are far enough from the rest of the points in the plot so as to disentangle them from a given data sample.

Thus, the abundance data from DLA objects are easily reproduced by models of massive galaxies with strong star formation in the early stages of their evolution. This evolution is so rapid in those galaxies that 300 Myr after the beginning of the formation of stars, the value of $\log(\text{N}/\text{O})$ increases from -2.5 to -1.6 with oxygen abundances $12 + \log(\text{O}/\text{H}) = 7\text{--}8.5$. Therefore, it should be possible to find objects in this zone of the N/O–O/H plot, although, given the shortness of this phase, the number of these objects would be small. We note that a level of $\log(\text{N}/\text{O}) \sim -1.6$ dex is easily reached in such a short time, in galactic evolutionary terms, as $t \sim 300$ Myr, even with a primary contribution coming from LIM stars.

5 CONCLUSIONS

The evolutionary track followed by a given region or galaxy in the N/O–O/H plane depends strongly on the star formation history of the region. Strong bursting star formation histories would produce high oxygen abundances soon and, hence, an early secondary behaviour, thus reproducing most of the spiral H II region observations. In contrast, a low and continuous SFR keeps the oxygen abundance low for a long time; thus, a large quantity of the NP may be ejected reproducing the flat slope shown by dwarf galaxy data.

The resulting dispersion of our realizations, similar to the one observed, appears as a consequence of the different star formation histories in each modelled region and in each galaxy. These are obtained by combining various star and molecular cloud formation efficiencies and collapse time-scales.

The stellar yields for LIM also play a role: if they have an adequate contribution of the NP depending on metallicity, it is easy to reproduce adequately the generic trend of the observational points in the N/O–O/H plane, in particular a flat slope for low-metallicity regions and, simultaneously, lower values of N/O at similar oxygen abundances for regions or galaxies where the star formation is strong and occurred early in the evolution.

The combination of the new yield set from GAV05 and the self-consistent chemical evolution models by Moll  & D  az (2005) is able to reproduce the data corresponding to H II regions in different galaxies and Galactic stars of different ages. This arises naturally just by assuming different input parameters (mostly star formation efficiencies and infall rates) for the different galaxies and regions in the same generic model, without the need to appeal to ad hoc models to reproduce each kind of object.

They may also be able to reproduce the existing data on galaxies at $0 \leq z \leq 4$, and predict the existence of a *second plateau*, found in the N/O–O/H relationship for $\log(\text{N}/\text{O}) \sim -2.5$ and galaxies with $z \geq 3$. Our models predict that objects at redshifts $z \leq 2.5$ cannot be discriminated from $z = 0$ objects in the $\log(\text{N}/\text{O})$ – $\log(\text{O}/\text{H})$ plane; however, for $z \geq 3$ objects, this discrimination is possible. This characteristic is a consequence of the rapid passage of model results by this zone of the plane, when the time-evolution is considered, since 300 Myr after the beginning of the formation of stars, the value $\log(\text{N}/\text{O})$ increases from -2.5 to -1.6 with oxygen abundances $12 + \log(\text{O}/\text{H}) = 7\text{--}8.5$.

ACKNOWLEDGMENTS

This work has been partially supported by the Spanish PNAYA project AYA2004–8260-C03. We acknowledge their comments to R. B. C. Henry and L. Pilyugin for their comment on the first version of this manuscript. We thank an anonymous referee for the useful comments and suggestions that have improved this paper.

REFERENCES

- Allain D., Collin-Souffrin S., Joly M., Vigroux L., 1979, A&A, 78, 200
- Barb  y B., 1983, A&A, 123, 1
- Burkert A., Hensler G., 1987, Lecture Notes in Physics Vol. 287. Springer-Verlag, Berlin, p. 159
- Cair  s L. M., Garc  a-Lorenzo B., Caon N., V  lchez J. M., Papaderos P., Noeske K., 2003, Ap&SS, 284, 611
- Carbon D. F., Barb  y B., Kraft R. P., Friel E. D., Suntzeff N. B., 1987, PASP, 99, 335
- Carigi L., Peimbert M., Esteban C., Garc  a-Rojas J., 2005, ApJ, 623, 213
- Castellanos M., D  az A. I., Terlevich E., 2002, MNRAS, 329, 315
- Centuri  n M., Molaro P., Vladilo G., P  roux C., Levshakov S. A., D’Odorico V., 2003, A&A, 403, 55
- Chiappini C., Matteucci F., Meynet G., 2003, A&A, 410, 257 (CHIA)
- Chiappini C., Matteucci F., Ballero S. K., 2005, A&A, 437, 429
- Chiappini C., Hirschi R., Meynet G., Ekstr  m S., Maeder A., Matteucci F., 2006, A&A, 449, L27
- Clegg R. E. S., Tomkin J., Lambert D. L., 1981, ApJ, 250, 262
- Contini T., Treyer M. A., Sullivan M., Ellis R. S., 2002, MNRAS, 330, 75
- Daflon S., Cunha K., 2004, ApJ, 617, 1115
- Dekel A., Woo J., 2003, MNRAS, 344, 1131
- Dray L. M., Tout C. A., Karakas A. I., Lattanzio J. C., 2003, MNRAS, 338, 973
- Edmunds M. G., Pagel B. E. J., 1978, MNRAS, 185, 77P
- Esteban C., Peimbert M., Torres-Peimbert S., Garc  a-Rojas J., Rodr  guez M., 1999a, ApJS, 120, 113
- Esteban C., Peimbert M., Torres-Peimbert S., 1999b, A&A, 342, L37

- Esteban C., Peimbert M., Torres-Peimbert S., García-Rojas J., 1999c, *Rev. Mex. Astron. Astrofis.*, 35, 65
- Ferrini F., Matteucci F., Pardi C., Penco U., 1992, *ApJ*, 387, 138
- Ferrini F., Mollá M., Pardi M. C., Díaz A. I., 1994, *ApJ*, 427, 745
- Fich M., Silkey M., 1991, *ApJ*, 366, 107
- Garnett D. R., 2002, *ApJ*, 581, 1019
- Garnett D. R., Skillman E. D., Dufour R. J., Peimbert M., Torres-Peimbert S., Terlevich R., Terlevich E., Shields G. A., 1995, *ApJ*, 443, 64
- Garnett D. R., Shields G. A., Peimbert M., Torres-Peimbert S., Skillman E. D., Dufour R. J., Terlevich E., Terlevich R. J., 1999, *ApJ*, 513, 168
- Gavilán M., Buell J. F., Mollá M., 2005, *A&A*, 432, 861 (GAV05)
- Gavilán M., Mollá M., Buell J. F., 2006, *A&A*, 450, 509 (GAV06)
- Gratton R. G., Sneden C., Carretta E., Bragaglia A., 2000, *A&A*, 354, 169
- Grimes J. P., Heckman T., Strickland D., Ptak A., 2005, *ApJ*, 628, 187
- Gummersbach C. A., Kaufer A., Schaefer D. R., Szeifert T., Wolf B., 1998, *A&A*, 338, 881
- Henry R. B. C., Edmunds M. G., Köppen J., 2000, *ApJ*, 541, 660 (HEN)
- Hensler G., Theis C., Gallagher J. S. I., 2004, *A&A*, 426, 25
- Hirschi R., 2005, in Hill V., François P., Primas F., eds, *Proc. IAU Symp.* 228, *From Lithium to Uranium: Elemental Tracers of Early Cosmic Evolution*. Cambridge Univ. Press, Cambridge, p. 331
- Israelian G., Ecuivillon A., Rebolo R., García-López R., Bonifacio P., Molaro P., 2004, *A&A*, 421, 649
- Izotov Y. I., Thuan T. X., 1999, *ApJ*, 511, 639
- Izotov Y. I., Thuan T. X., Guseva N. G., 2005, *ApJ*, 632, 210
- Laird J. B., 1985, *ApJ*, 289, 556
- Lanfranchi G. A., Friaça A. C. S., 2003, *MNRAS*, 343, 481
- Larsen T. I., Sommer-Larsen J., Pagel B. E. J., 2001, *MNRAS*, 323, 555
- Legrand F., 2000, *A&A*, 354, 504
- Marcolini A., Brighenti F., D'Ercole A., 2004, *MNRAS*, 352, 363
- Marigo P., Bressan A., Chiosi C., 1998, *A&A*, 331, 564
- McCall M. L., Rybski P. M., Shields G. A., 1985, *ApJS*, 57, 1
- Meynet G., Maeder A., 2002, *A&A*, 390, 561
- Mollá M., Díaz A. I., 2005, *MNRAS*, 358, 521
- Mollá M., Ferrini F., Díaz A. I., 1996, *ApJ*, 466, 668
- Mouhcine M., Contini T., 2002, *A&A*, 389, 106
- Nava A., Casebeer D., Henry R. B. C., Jevremovic C. D., 2006, *ApJ*, 645, 1076
- Ott J., Walter F., Brinks E., 2005, *MNRAS*, 358, 1453
- Pagel B. E. J., Edmunds M. G., Blackwell D. E., Chun M. S., Smith G., 1979, *MNRAS*, 189, 95
- Peimbert M., 1979, in Burton W. B., ed., *Proc. IAU Symp.* 84, *The Large-Scale Characteristics of the Galaxy*. Reidel, Dordrecht, p. 307
- Pettini M., Ellison S. L., Bergeron J., Petitjean P., 2002, *A&A*, 391, 21
- Pilyugin L. S., 2004, *A&A*, 423, 427
- Pilyugin L. S., Thuan T. X., Vilchez J. M., 2003, *A&A*, 397, 487
- Portinari L., Chiosi C., Bressan A., 1998, *A&A*, 334, 505
- Prantzos N., 2003, in Charbonnel C., Schaerer D., Meynet G., eds, *ASP Conf. Ser.* Vol. 304, *CNO in the Universe*. Astron. Soc. Pac., San Francisco, p. 361 (PRAN)
- Prochaska J. X., Henry R. B. C., O'Meara J. M., Tytler D., Wolfe A. M., Kirkman D., Lubin D., Suzuki N., 2002, *PASP*, 114, 933
- Rasmussen J., Stevens I. R., Ponman T. J., 2004, *MNRAS*, 354, 259
- Recchi S., Hensler G., 2006, *A&A*, 445, L39
- Recchi S., Hensler G., Angeretti L., Matteucci F., 2006, *A&A*, 445, 875
- Renzini A., Voli M., 1981, *A&A*, 94, 175
- Romano D., Tosi M., Matteucci F., 2006, *MNRAS*, 365, 759
- Schaller G., Schaerer D., Meynet G., Maeder A., 1992, *A&AS*, 96, 269
- Serrano A., 1986, *PASP*, 98, 1066
- Shaver P. A., McGee R. X., Newton L. M., Danks A. C., Pottasch S. R., 1983, *MNRAS*, 204, 53
- Smartt S. J., Venn K. A., Dufton P. L., Lennon D. J., Rolleston W. R. J., Keenan F. P., 2001, *A&A*, 367, 86
- Spite M. et al., 2005, *A&A*, 430, 655
- Thuan T. X., Izotov Y. I., 2005, *ApJ*, 627, 739
- Thuan T. X., Izotov Y. I., Lipovetsky V. A., 1995, *ApJ*, 445, 108
- Tinsley B. M., 1980, *Fundam. Cosmic Phys.*, 5, 287
- Tolstoy E., 2003, *Ap&SS*, 284, 579
- Tomkin J., Lambert D. L., 1984, *ApJ*, 279, 220
- Tsamis Y. G., Barlow M. J., Liu X.-W., Danziger I. J., Storey P. J., 2003, *MNRAS*, 338, 687
- van den Hoek L. B., Groenewegen M. A. T., 1997, *A&AS*, 123, 305
- van Zee L., Haynes M. P., 2006, *ApJ*, 636, 214
- van Zee L., Salzer J. J., Haynes M. P., O'Donoghue A. A., Balonek T. J., 1998, *AJ*, 116, 2805
- van Zee L., Barton E. J., Skillman E. D., 2004, *AJ*, 128, 2797
- van Zee L., Skillman E. D., Haynes M. P., 2006, *ApJ*, 637, 269
- Veilleux S., Cecil G., Bland-Hawthorn J., 2005, *ARA&A*, 43, 769
- Vila Costas M. B., Edmunds M. G., 1993, *MNRAS*, 265, 199
- Vilchez J. M., Esteban C., 1996, *MNRAS*, 280, 720
- Woosley S. E., Weaver T. A., 1986, *Lecture Notes in Physics* Vol. 255. Springer-Verlag, Berlin, p. 91
- Woosley S. E., Weaver T. A., 1995, *ApJS*, 101, 181 (WW)

This paper has been typeset from a $\text{\TeX}/\text{\LaTeX}$ file prepared by the author.